Transitions in synchronization states of model cilia through basal-connection coupling

Yujie Liu[1], Rory Claydon[2], Marco Polin[2,3†], and Douglas R. Brumley[1*]
[1] *School of Mathematics and Statistics, The University of Melbourne, Victoria 3010, Australia.*
[2] *Physics Department, University of Warwick, Gibbet Hill Road, Coventry CV4 7AL, UK.*
[3] *Centre for Mechanochemical Cell Biology, University of Warwick, Gibbet Hill Road, Coventry CV4 7AL, UK.*

Despite evidence for a hydrodynamic origin of flagellar synchronization between different eukaryotic cells, recent experiments have shown that in single multi-flagellated organisms, coordination hinges instead on direct basal body connections. The mechanism by which these connections leads to coordination, however, is currently not understood. Here we focus on the model biflagellate *Chlamydomonas reinhardtii*, and propose a minimal model for the synchronization of its two flagella as a result of both hydrodynamic and direct mechanical coupling. A spectrum of different types of coordination can be selected, depending on small changes in the stiffness of intracellular couplings. These include prolonged in-phase and anti-phase synchronization, as well as a range of multistable states induced by spontaneous symmetry breaking of the system. Linking synchrony to intracellular stiffness could lead to the use of flagellar dynamics as a probe for the mechanical state of the cell.

INTRODUCTION

Cilia and flagella are structurally identical, whip-like cellular organelles employed by most eukaryotes for tasks ranging from sensing and locomotion of single cells [1], to directing embryonic development [2] and driving cerebrospinal fluid flow [3] in animals. Originally observed in 1677 by the Dutch pioneer Antoni van Leeuwenhoek, groups of motile cilia and flagella have a seemingly spontaneous tendency to coordinate their beating motion and generate large-scale patterns known as metachronal waves [4]. Coordination has often been proposed to provide an evolutionary advantage by improving transport and feeding efficiency [5–10], although estimates of the magnitude of this effect are notoriously difficult. Despite the uncertainty on its biological role, however, the universality of flagellar coordination is an empirical fact, and it suggests the existence of a correspondingly general mechanism for synchronization. Mechanical forces, transmitted either by the surrounding fluid or internally through the cells, have often been proposed as responsible for this coordination [11–15]. Understanding how synchronization emerges could therefore highlight novel and potentially subtle roles played by physical forces in cell biology. Here we develop a minimal model that links small changes in the mechanical properties of cells with the dynamics of their protruding flagella. In turn, this approach could lead to coordination being used as a probe to measure the internal mechanical state of a cell.

Reports of coordinated motion in nearby swimming sperm [16, 17] hint at the importance of hydrodynamic coupling. Hydrodynamic-led coordination of self-sustained oscillators, mimicking the active motion of cilia and flagella [18, 19], has been extensively investigated theoretically [12, 20–22], numerically [23–25], and experimentally with colloidal rotors [26, 27] and rowers [28, 29]. Despite the peculiar constraints of low-Reynolds number hydrodynamics, these studies suggest that hydrodynamic interactions can lead to ciliary coordination when coupled to either a phase-dependent driving force [12, 21], or axonemal elasticity [30]. Indeed, hydrodynamic-mediated synchronization has been confirmed experimentally between pairs of eukaryotic flagella from different somatic cells from the green alga *Volvox carteri* [14].

Inter-cellular coordination of flagella, however, does not necessarily imply intra-cellular coordination, and therefore it is not *a priori* clear whether hydrodynamic coupling is also responsible for the synchronization observed in individual multi-flagellated cells. Experimental studies of flagellar coordination within a single cell have focussed mainly on the biflagellate green alga *Chlamydomonas reinhardtii* [31, 32] (CR), whose flagella are usually locked in a characteristic in-phase breaststroke motion. Early studies of flagellar coordination in CR [33–35] were recently refined [11, 36] and extended [37] using microfluidic devices and high-speed imaging of flagella [38]. These pointed at a fundamentally hydrodynamic origin for the observed synchronization, either through direct coupling or *via* a mechanism based on cell-body rocking [13]. However, a series of elegant novel experiments in CR and other flagellates challenged this view convincingly, showing instead that coordination requires the intracellular striated fibres that join flagellar basal bodies [39, 40]. For the CR mutant *vfl3*, with impaired mechanical coupling and a variable number of flagella, synchronization is completely disrupted [39] except for sporadic periods of synchrony in cells with two close flagella oriented in the same direction (see Fig. S1 in [40]). Even though the precise mechanism by which direct connections affect flagellar coordination remains to be clarified [15], the spontaneous transitions between extended in-phase (IP) and anti-phase (AP) beating in the CR mutant *ptx1* [41], already suggest that multiple synchronization states should be achievable through changes in the fibres' mechanical properties within the physiological range.

Here we propose a minimal model for flagellar dynamics for CR which can sustain both stable IP and stable

* d.brumley@unimelb.edu.au, † m.polin@warwick.ac.uk

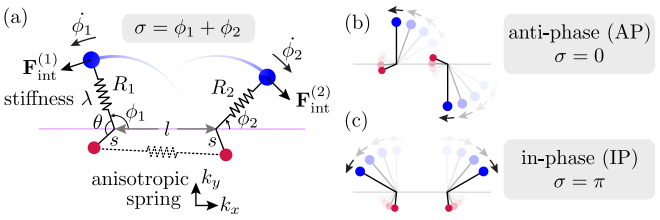

FIG. 1. Physical configuration. (a) Two external rotors (blue), moving in the fluid, mimic the beating motion of flagellar filaments. Internal rotors (red) represent the flagellar basal bodies, and are coupled through an anisotropic spring. (b) Anti-phase (AP) and (c) in-phase (IP) states.

AP states even in the absence of hydrodynamic coupling. Within this framework, the phase dynamics are determined principally by the mechanical state of the basal body fibres [42], with both types of coordination possible within a physiological range of fibres' stiffnesses [43]. The inclusion of hydrodynamic coupling leads to the emergence of a region in parameter space where non-trivial states can emerge as a result of spontaneous symmetry breaking through pitchfork bifurcations of limit cycles.

I. MINIMAL MODEL AND LEADING ORDER DYNAMICS

Figure 1a summarises our minimal model of flagella coupled through hydrodynamic and basal-body interactions. Following previous theoretical work [20, 44], and experimental measurements of flagellar flow fields and waveform elasticity [14], the two flagella of *Chlamydomonas* are represented here by two spheres of radius a, immersed in a three dimensional fluid of viscosity μ, and driven around circular orbits of radii R_i $(i = 1, 2)$ by constant tangential driving forces $\mathbf{F}^{(i)}_{\rm int}$. Springs of stiffness λ resist radial excursions from the equilibrium length R_0; and the magnitude of the internal driving forces, $F^{(i)}_{\rm int} = 6\pi\mu a R_0\,\omega_i$ guarantees that, when isolated, the i-th oscillator will rotate at the intrinsic angular speed ω_i. The orbits are centred along the x-axis, a distance l apart, and lie along the xy plane. Polar and radial coordinates (ϕ_i, R_i) define the oscillators' instantaneous positions around the centres of their respective orbits. We will refer to $R_i(t)$ as the external rotor radii.

Both hydrodynamic and direct elastic interactions couple these minimal cilia. Hydrodynamic coupling is mediated by the fluid disturbance generated by each sphere's motion, modelled here as the flow from a point force. These interactions affect the instantaneous angular speeds $\dot\phi_i$ both directly, through a hydrodynamic torque, and indirectly by modifying the orbits' radii. For counter-rotating oscillators like those describing *Chlamydomonas* flagella, the resulting effective coupling will promote AP synchronization [15, 41, 44, 45] (Fig. 1b). In addition to external flagellar interactions, considerable evidence [39, 40] suggests that flagellar dynamics are strongly influenced by direct intracellular mechanical coupling, through striated fibres joining the basal bodies [33, 46] that can lead the system to IP synchrony (Fig. 1c). Intracellular connections are modelled here by introducing, for each oscillator, an auxiliary arm of fixed length s ($\ll R_0$) at an angle θ ahead of the rotating sphere. The endpoints of these arms (red spheres in Fig. 1a) are coupled via an *anisotropic* elastic medium acting as elastic springs of stiffnesses (k_x, k_y) and equilibrium lengths $(l, 0)$ in the x and y directions respectively. This is intended to represent the intrinsically anisotropic structure of the fibre bundles connecting the basal bodies [42]. The equations of motion, derived in Supplementary Information S1, follow from the requirement of zero net force and torque on each oscillator, and in the limit $R_0/l \ll 1$ can be approximated as (see Supplementary Information S1)

$$
\begin{aligned}
\dot\phi_1 &= \frac{R_0}{R_1}\omega_1 + \rho\frac{R_2}{R_1}\dot\phi_2 J(\phi_1,\phi_2) + \rho\frac{\dot R_2}{R_1}K(\phi_1,\phi_2)\\
&+ \frac{s^2}{\zeta R_1^2}(k_x+k_y)\left[G(\phi_1+\theta,\phi_2-\theta) - G(\phi_1+\theta,\phi_1+\theta)\right]\\
\dot\phi_2 &= \frac{R_0}{R_2}\omega_2 + \rho\frac{R_1}{R_2}\dot\phi_1 J(\phi_2,\phi_1) + \rho\frac{\dot R_1}{R_2}K(\phi_2,\phi_1)\\
&+ \frac{s^2}{\zeta R_2^2}(k_x+k_y)\left[G(\phi_2-\theta,\phi_1+\theta) - G(\phi_2-\theta,\phi_2-\theta)\right]\\
\dot R_1 &= -\frac{\lambda}{\zeta}(R_1-R_0) + \rho R_2\dot\phi_2 K(\phi_2,\phi_1) + \rho\dot R_2 H(\phi_1,\phi_2)\\
\dot R_2 &= -\frac{\lambda}{\zeta}(R_2-R_0) + \rho R_1\dot\phi_1 K(\phi_1,\phi_2) + \rho\dot R_1 H(\phi_2,\phi_1)
\end{aligned}
\tag{1}
$$

where $\rho = 3a/8l$ ($\rho \ll 1$ as $a \lesssim R_0$); $\zeta = 6\pi\mu a$ is the viscous drag coefficient of the rotating sphere; and

$$
\begin{aligned}
J(a,b) &= 3\cos(a-b) - \cos(a+b),\\
K(a,b) &= -3\sin(a-b) - \sin(a+b),\\
H(a,b) &= 3\cos(a-b) + \cos(a+b),\\
G(a,b) &= \frac{1}{2}\frac{k_y-k_x}{k_x+k_y}\sin(a+b) - \frac{1}{2}\sin(a-b).
\end{aligned}
\tag{2}
$$

In order to model the configuration typical of *Chlamydomonas* we will focus here on identical but counter-rotating oscillators, $\omega_1 = -\omega_2 = \omega$. Parameter values are given in Table I unless otherwise specified.

II. FIBRES-ONLY COUPLING

Despite the apparent simplicity, this minimal system displays rich dynamics, and it is therefore convenient to analyse its behaviour following steps of increasing complexity. Let us begin by considering the case in which hydrodynamic coupling is completely neglected. The hydrodynamic drag is still necessary for each model cilium

Variable	*Symbol*	*Value*
model cilium radius [14]	a	0.75 μm
interflagellar spacing	l	15 μm
int./ext. rotor angle	θ	0
equilibrium external rotor radius	R_0	5 μm
fixed internal rotor radius	s	0.1 μm
external spring stiffness [22]	λ	4×10^{-7} Nm^{-1}
viscosity of water	μ	10^{-3} Pa s
ciliary beat frequency [11]	$f=\omega/2\pi$	50 Hz

TABLE I. Minimal model parameters used throughout, unless stated otherwise.

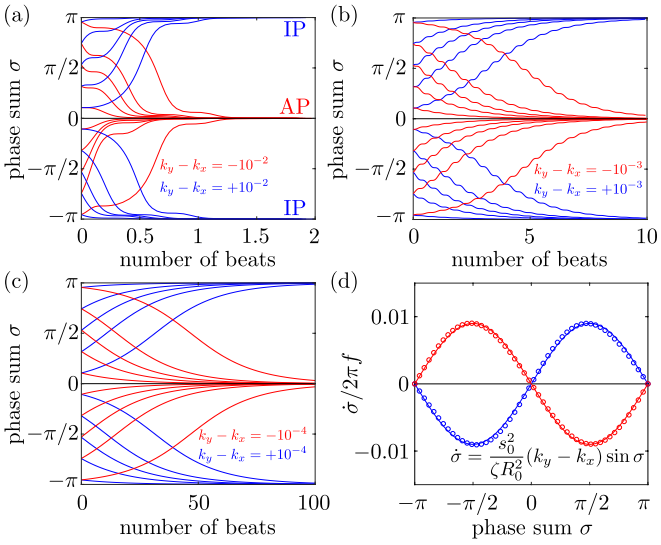

FIG. 2. Synchronization dynamics for pairs of model cilia in the absence of hydrodynamic interactions. Phase sum, $\sigma(t)=\phi_1(t)+\phi_2(t)$, for (a) $k_y-k_x=\pm10^{-2}$ Nm^{-1}, (b) $k_y-k_x=\pm10^{-3}$ Nm^{-1} and (c) $k_y-k_x=\pm10^{-4}$ Nm^{-1}. In each case (starting with $\phi_1(0)=0$), IP (blue) and AP (red) synchronized states are obtained for $k_y>k_x$ and $k_y<k_x$, respectively, over a time-scale inversely proportional to $\max(k_y,k_x)$. (d) Values of $\dot\sigma(\sigma)$ measured from numerical simulations (circles) compare favourably with Eq. (4) for sufficiently soft internal springs. Other model parameters as given in Table I.

(through ζ) in order to balance the driving force, but there is no direct hydrodynamic coupling between the spheres. In this case $R_1=R_2=R_0$, and recasting the angular dynamics in terms of phase sum and difference $(\sigma,\delta)=(\phi_1+\phi_2,\phi_1-\phi_2)$ we obtain

$$\dot\sigma=(k_y-k_x)\frac{2s^2}{\zeta R_0^2}\sin^2\left(\frac{\delta}{2}+\theta\right)\sin(\sigma), \tag{3}$$

$$\dot\delta=2\omega-\frac{s^2}{\zeta R_0^2}\left[(k_y+k_x)+(k_y-k_x)\cos(\sigma)\right]\sin(\delta+2\theta).$$

Requiring that the maximal torque exerted on each oscillator by the internal springs is always smaller than that from the driving force ($\max(k_x,k_y)s^2<\zeta R_0^2\omega$) guarantees that the cilia will always be beating ($\dot\delta>0$), and defines a physiologically plausible range for k's, which in our case is $k_{x,y}\lesssim10^{-2}$ Nm^{-1}. At the same time, unless $k_x=k_y$, the system will monotonically converge to either IP ($\sigma=\pi$) or AP ($\sigma=0$) synchrony, depending on whether k_y is larger or smaller than k_x. Figure 2a-c shows the convergence to either state, for a set of initial conditions and increasing internal stiffnesses. When $k_{x,y}\lesssim10^{-3}$ Nm^{-1}, the phase sum evolves much faster than the difference, and σ follows the approximate dynamics

$$\dot\sigma=(k_y-k_x)\frac{s^2}{\zeta R_0^2}\sin(\sigma), \tag{4}$$

as shown in Fig. 2d. The instantaneous and average phase speed profile can be solved analytically (see Supplementary Information S3). In the case of k_x (in IP) $>$ k_y (in AP), the model predicts a lower average phase speed in IP than in AP which is in qualitative agreement with experimental observations [41]. Recent studies argue that hydrodynamics plays a negligible role in flagellar synchronization for single cells [39, 40]. Without hydrodynamics, our model predicts that the effective interflagellar coupling should be given by $2\pi\epsilon=\kappa s^2/\omega\zeta R_0^2$. Using the known value for *Chlamydomonas*, $|\epsilon|\simeq0.015$ [11, 41], we obtain $\kappa\simeq10^{-3}$ Nm^{-1}. The Young's modulus for the bundle of striated fibres can then be estimated, $E=\kappa L/A$, where L and A are the length and cross-sectional area of the bundle, respectively. Taking $L=250$ nm and $A=\pi\cdot25^2$ nm^2 results in the value $E\simeq10^5$ Pa [42, 47]. This is a biologically plausible estimate, midway between the elastic modulus of relaxed skeletal muscle ($E\sim10^4$ Pa) and elastin ($E\sim10^6$ Pa) [43].

III. STIFF FLAGELLA HYDRODYNAMICS

We begin now to include the effect of hydrodynamic interactions under the assumption of artificially stiff flagella, implemented in this section by increasing the radial spring stiffness to $\lambda=4\times10^{-6}$ Nm^{-1} (10× the value in Table I). Increasing λ reduces the typical response time of the radial coordinate (ζ/λ) and, when this is much smaller than the angular timescale ($2\pi/\omega$), it allows us to simplify the dynamics by assuming an instantaneous radial response [44]. Then, to first order in the small parameter ρ, Eqs. (1) imply that σ will obey

$$\dot\sigma=\left[(k_y-k_x)\frac{s^2}{\zeta R_0^2}-\frac{2\rho\omega^2\zeta}{\lambda}\right]\sin(\sigma), \tag{5}$$

once the dynamics have been averaged over the fast variable δ. The coefficient of $\sin(\sigma)$ above provides an intuitive understanding of the roles of basal body coupling and elasto-hydrodynamic interactions in determining the synchronization state of the system, which is useful as a general rule of thumb to assess the relative importance of these phenomena even beyond the "stiff flagella" case.

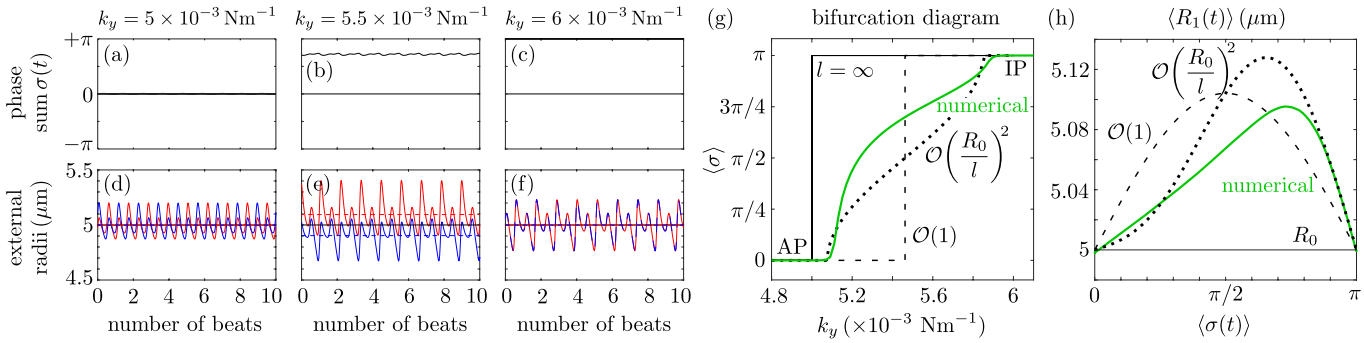

FIG. 3. Steady state solutions when radial dynamics are fast compared to the phase dynamics. This is achieved by setting $\lambda = 10\lambda_0 = 4 \times 10^{-6}$ Nm^{-1}. In each simulation $k_x = 5 \times 10^{-3}$ Nm^{-1}. Other parameters shown in Table I. (a-c) Phase sum $\sigma(t) = \phi_1(t) + \phi_2(t)$ and (d-f) external rotor radii $R_i(t)$ are shown as functions of time for various values of k_y. (g) The mean value of phase sum, $\langle\sigma(t)\rangle$ and (h) external rotor radius $R_1(t)$ are computed from numerical solutions (green) and compared with analytical predictions of Eq. (5) (dashed) and Eqs. (6,7) (dotted).

Within this approximation, hydrodynamics appears to simply shift the location of the transition between AP and IP states, determined by the steady state time average $\langle\sigma\rangle$, from $k_y = k_x$ to $k_y = k_x + 2\rho(R_0/s)^2(\omega\zeta/\lambda)^2\lambda$. This is indeed confirmed by simulations of the full system for large l (see Fig. 4b).

A closer inspection, however, reveals more intriguing dynamics which become particularly evident for small inter-flagellar separations. Figure 3a-c shows the steady state dynamics of σ for $l = 15\,\mu$m, as k_y is swept across the transition. Between AP and IP coordination (Figs. 3a,c) there is a distinct region of k_y-values for which the system synchronizes in a non-trivial intermediate state (Fig. 3b). This is accompanied by a permanent difference in the average values of the oscillators' radii (Fig. 3e), with the asymmetry depending on which of the equally probable signs of $\langle\sigma\rangle$ is chosen by the system. Figure 3g shows the full positive branch of $\langle\sigma\rangle$ as k_y is swept between AP and IP values (simulations: green solid line). This can be compared to the leading-order behaviour with and without hydrodynamics (black dashed and solid lines); and the one predicted by refining Eq. (5) to next-to-leading order in R_0/l (black dotted line; see Supplementary Information S2)

$$\dot{\sigma} = \left[(k_y - k_x)\frac{s^2}{\zeta R_0^2} - \frac{2\rho\omega^2\zeta}{\lambda}\left(1 - \frac{15}{2}\frac{R_0^2}{l^2}\cos(\sigma)\right)\right]\sin(\sigma). \tag{6}$$

The semi-quantitative agreement between the simulated and predicted dependence of the steady-state $\langle\sigma\rangle$ extends also to the k_y-dependence of the time-averaged radii (Fig. 3h), which follows in the same approximation

$$R_{1,2} = R_0\left[1 \pm \frac{\rho\omega\zeta}{\lambda}\left(1 - \frac{15}{2}\frac{R_0^2}{l^2}\cos(\sigma)\right)\sin(\sigma)\right]. \tag{7}$$

Figure 4a shows that the agreement extends across the full range of separations $l \geq 15\,\mu$m, with particularly accurate estimates for the values of k_y marking the beginning and end of the transition (Fig. 4b). These results suggest that the simple expression in Eq. (6) captures the essential features of the dynamics, and can therefore be used to analyse the nature of the transition. For small deviations δk in k_y around the transition from AP, Eq. (6) can be approximated as

$$\dot{\sigma} \simeq \left(\delta k\frac{s^2}{\zeta R_0^2}\right)\sigma - \left(\frac{15}{2}\frac{\rho\omega^2\zeta}{\lambda}\frac{R_0^2}{l^2}\right)\sigma^3, \tag{8}$$

which therefore suggests that the emergence of non-trivial coordination follows a supercritical pitchfork bifurcation [48]. A similar argument leads to an equivalent conclusion for the bifurcation from IP as k_y is decreased. AP and IP domains are therefore bounded by a pitchfork bifurcation of limit cycles.

Within the intermediate regime, the system becomes naturally bistable through a spontaneous symmetry breaking from a state where both oscillators follow the same limit cycle to one where they sustain a stable difference in their average oscillation amplitudes (see Fig. 3e). Transitions between homogeneous and inhomogeneous oscillation states, and bistability, have only recently been discovered in pairs of coupled limit cycle oscillators, also as a consequence of non-equilibrium symmetry-breaking pitchfork bifurcations [49, 50]. Here we discover their emergence in a simple model of hydrodynamic- and basal-body-coupled flagella. Intermediate equilibrium states appear when the internal elastic interaction promoting IP coordination is approximately compensated by the leading order hydrodynamic coupling favouring AP, amplifying the importance of higher-order hydrodynamic effects. In this parameter range, the oscillators are able to sustain a stable difference in their average amplitude (external rotor radii). Interestingly, the permanent difference in the average radii of the two oscillators after the bifurcation could be easily interpreted by an observer as a difference in intrinsic frequency (since $\omega \propto 1/R_0$). The rotors would then appear intrinsically different despite in fact being identical. Eventually, a sufficient increase of the internal stiffness can overcome the antagonistic effect

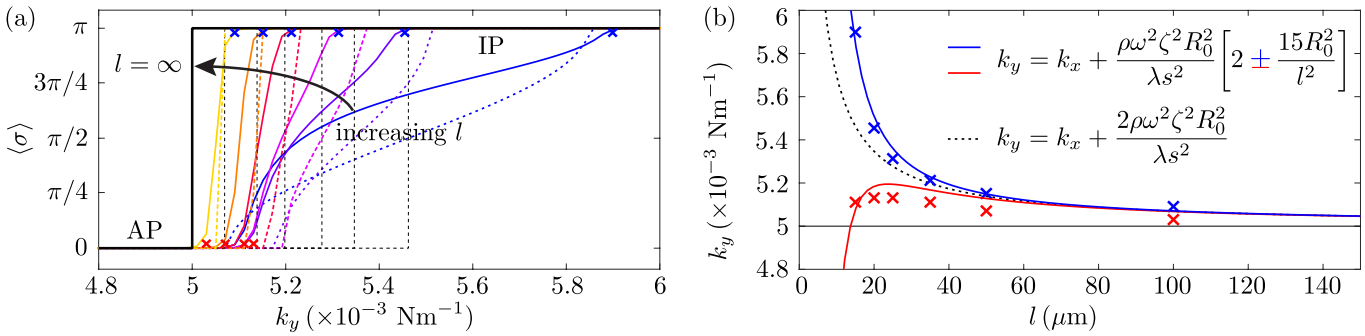

FIG. 4. Transitions between synchronization states mediated by basal body coupling. Radial dynamics are again fast compared to phase dynamics ($\lambda = 10\times\lambda_0 = 4\times10^{-6}$ Nm^{-1}). (a) Steady state $\langle\sigma(t)\rangle$ as a function of k_y for various ciliary spacings (l = 15, 20, 25, 35, 50, 100 μm). Numerical solutions (smooth, coloured) are shown alongside analytical predictions to leading order (dashed, black) and second order in R_0/l (dashed, coloured). The transition zone boundaries are quantified by $\langle\sigma(t)\rangle = 0.02\pi$ (red crosses) and $\langle\sigma(t)\rangle = 0.98\pi$ (blue crosses) respectively. (b) These are shown as a function of l, together with leading order (black) and second order in R_0/l (coloured) analytical predictions.

of hydrodynamic interactions at any given separation l, and drive the system to a stable IP state.

IV. THE FULL MODEL

We conclude by looking at the full system with realistic parameters throughout (see Table I). In this case, radial and phase dynamics have comparable timescales ($\zeta\omega/2\pi\lambda \sim 2$) and the radii cannot be considered as approximately slaved to the phases anymore. Together with the sizeable radial deformations ($\delta R/R_0 \sim R_0/2l$ here and ~ 0.2 for *Chlamydomonas*-like $l = 15\,\mu$m) this results in a complex interplay between radial and phase variables, and implies the need to consider the full system of governing equations (see Supplementary Information S1). These will be explored here through numerical simulations only.

Figure 5a,b shows a representative set of curves for a k_y sweep with $k_x = 5\times10^{-3}\,$Nm^{-1} and $l = 15\,\mu$m. Supplementary movies 1–5 show the dynamics for panels (i)–(v) respectively. Similarly to the case of stiffer flagella, low and high values of k_y correspond respectively to AP (panels (i)) and IP (panels (v)) synchronization, and in these states the oscillators follow the same dynamics. The average phase speed, however, is observed to be lower in IP than in AP (a difference of $\sim 13\%$ between $k_y = 0$ Nm^{-1} and $k_y = 0.02$ Nm^{-1}), in qualitative agreement with experimental observations of CR mutants [41] (see Supplementary Information S3). In between, there is a range of k_y values for which the system synchronizes around intermediate values of $\langle\sigma\rangle$, with the two oscillators following again different limit cycles (panels (iii,iv)). A new state, however, appears as k_y approaches the symmetry breaking transition from the AP side (panels (ii)). Despite corresponding formally to AP ($\langle\sigma\rangle = 0$), the system displays symmetric excursions in the relative phase difference which are long lived and not much smaller than π. In this state, the oscillators spend most of their time at values of σ far from 0, and the null average is only guaranteed by the symmetry of the dynamics. Although the system oscillates here by about $\pi/3$, amplitudes $\sim\pi$ can be easily obtained just by increasing a (Supplementary Information Fig. S2). In this condition the system will not appear synchronized in AP at all, but will rather be continuously alternating between IP at π and IP at $-\pi$. Figure 5c,e shows that this situation is typical for all of the separations displaying a discontinuous, rather than continuous, transition out of the AP state (here all $l \leq 35\,\mu$m). In the IP case, instead, the transition maintains its continuous nature throughout, and in fact the bifurcation point is still well predicted by the first order expression from Eq. (5) (see inset).

From the AP side, discontinuous transitions are always preceded by a region of k_y values where the system displays a large excursion dynamics, which therefore acts as a predictor of the impending discontinuity [51]. Figure 5e shows the variance, $\langle\sigma(t)^2\rangle - \langle\sigma(t)\rangle^2$, of the time-dependent signal, $\sigma(t)$, averaged over 7 seconds (> 300 beats). The large excursions evident in Fig. 5a(ii) manifest in the peak of Fig. 5e.

The presence of the discontinuity in $\langle\sigma\rangle$, and the preceding large fluctuations, depend on both the separation l and k_x, as shown in Fig. 6 for a (k_x, k_y) parameter sweep. For the realistic inter-flagellar separation ($l = 15\,\mu$m), Fig. 6a shows that the region of discontinuous transition out of AP, marked by the large standard deviation of $\sigma(t)$, exists only for $k_x \lesssim 9\times10^{-3}\,$Nm^{-1}. Above this value, the bifurcation changes its nature and becomes continuous but sharp. At the slightly larger separation of $l = 25\mu$m, the width of the extended transition zone observed previously for $k_x \lesssim 9\times10^{-3}\,$Nm^{-1} is reduced (see Figs. 6b, 5c). Further increasing the separation to $l = 100\,\mu$m reduces hydrodynamic forces by an order of magnitude compared to the $l = 15\,\mu$m case, and for all the k_x values explored, the system follows a sharp continuous transition from AP to IP as k_y is increased.

Although exploring in detail the nature of these bifur-

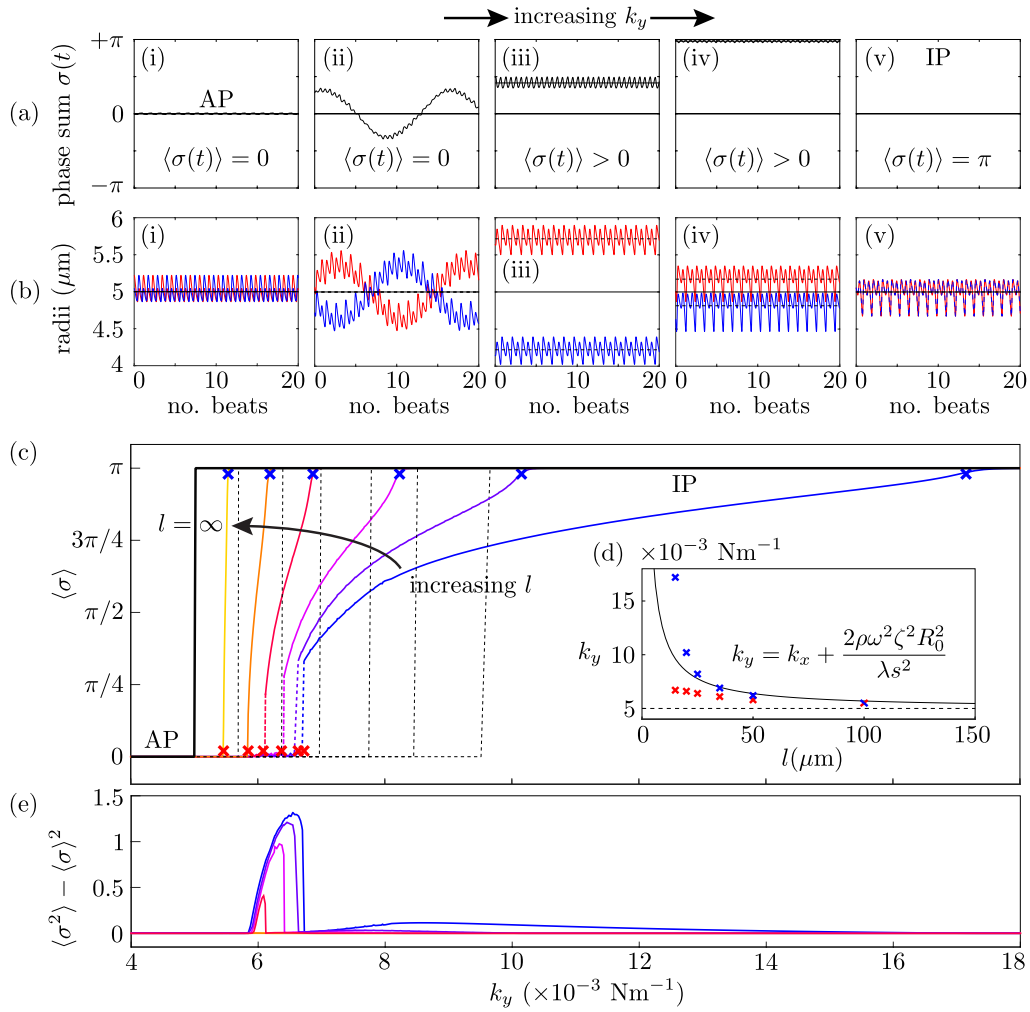

FIG. 5. Basal body coupling and hydrodynamic interactions. (a) Steady state phase sum $\sigma(t) = \phi_1(t) + \phi_2(t)$ and (b) external radii $R_1(t)$ and $R_2(t)$. Results are shown for k_y = 0.0055, 0.006, 0.007, 0.017, 0.020 Nm^{-1} with k_x = 0.005 Nm^{-1} and $l = 15\,\mu$m. For intermediate values of k_y, the external rotors possess a permanent difference in their intrinsic frequencies. Supplementary movies 1–5 show the dynamics for panels (i)–(v) respectively. (c) Value of $\langle\sigma(t)\rangle$ as a function of k_y for various values of l (results shown for l = 15, 20, 25, 35, 50, 100 μm). The transition zone boundaries are quantified by $\langle\sigma(t)\rangle = 0.02\pi$ (red crosses) and $\langle\sigma(t)\rangle = 0.98\pi$ (blue crosses) respectively; dashed black lines show far-field analytical predictions to leading order (from Eq. (5)). (d) Measured boundaries compared with leading-order far-field analytical results. (e) The variance of the time-dependent phase sum, $\langle\sigma(t)^2\rangle - \langle\sigma(t)\rangle^2$, for given values of k_y and l, reveals large excursions in the phase sum prior to the bifurcation (see panel (a)ii for the raw time-dependent signal).

cations is beyond the scope of the present work, clear similarities with the case of stiff flagella suggest strongly that the qualitative nature of the continuous transition is the same in the two cases. We expect therefore the continuous transitions to be supercritical pitchfork bifurcations of limit cycles, inducing the observed symmetry breaking in the system (Fig. 5a (iii-iv)). For $l \leq 35\,\mu$m, the emergence of a discontinuity in $\langle\sigma\rangle$ implies that decreasing k_x can change the nature of the transition. Looking closely at the discontinuous case, we find that there is an extended region of overlap between the $\langle\sigma\rangle = 0$ and the intermediate $\langle\sigma\rangle$ branches (see Supplementary Information S5). This is typical of a catastrophe-like transition which, given the $\sigma \leftrightarrow -\sigma$ symmetry of the system, is likely to be a subcritical pitchfork bifurcation.

Coexistence of three different states, all of which are locally stable for the dynamics, means that the system displays multi-stability: presence of noise might then induce the system to jump between these locally stable states and therefore alternate between periods of AP synchronization an other non-trivial types of coordination, with transitions dictated by escape rate arguments [52–54].

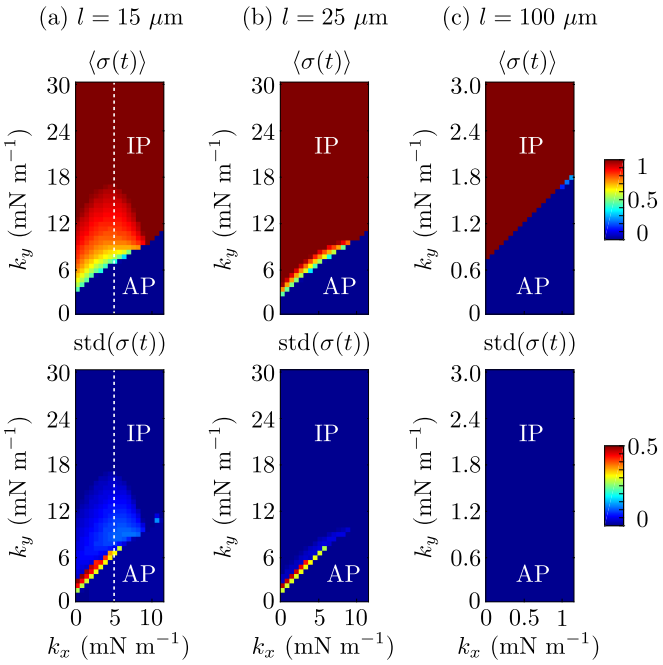

FIG. 6. Transition between AP and IP states is mediated by internal spring constants. Mean and standard deviation of $\sigma(t)$ as functions of k_x and k_y for external rotor separations (a) $l = 15$ μm, (b) $l = 25$ μm, and (c) $l = 100$ μm. White dotted lines correspond to the blue bifurcation plot in Fig. 5(c). For small k_x, the system is capable of supporting intermediate phase-locked states, with $0 < \langle\sigma(t)\rangle < \pi$. However, for larger k_x, an abrupt transition between AP and IP occurs.

V. CONCLUSIONS

While mechanisms for hydrodynamic-led synchronization of cilia and flagella have been extensively studied [12, 14, 20, 21, 23–27, 55], the impact of direct intracellular connections on flagellar dynamics is only starting to be recognised [15, 39, 40]. Here we have extended a simple and popular minimal model for the hydrodynamically interacting flagella pair of *Chlamydomonas* to account for intracellular mechanical coupling. The clearly anisotropic ultrastructure of striated fibres [42] is mirrored in the use of a non-isotropic elastic interaction between the oscillators ($k_x \neq k_y$), and results in a phase-phase coupling that can promote *by itself* either IP or AP synchronization, within a biologically plausible range of Young's moduli. Transitions would then result simply through changes in the relative magnitude of k_x and k_y. Given that intracellular calcium can control the contraction of striated fibres in *Chlamydomonas* [56], we hypothesise that the transitions in coordination observed experimentally could be the result of localised apical variations in cytoplasmic [Ca^{2+}] [57–59]. Natural extensions of this model to amplitude-phase coupling do not influence the leading order coordination dynamics (see Supplementary Information S1 for brief discussion) and have been omitted here. In-phase coordination has recently been proposed to result from a different nonlinear interplay between hydrodynamic and intracellular mechanical coupling [15], with AP due to either one of them operating in isolation. However, several experimental observations, from the absence of phase-locking in mutants lacking striated fibres [39, 40], to the complex synchronization observed in multi-flagellated algae [40], suggest that hydrodynamics plays in fact only a minimal role in this system. The model introduced here can sustain both AP and IP states without the need for external coupling, through a mechanism potentially under the direct control of the cell. Unequal tightening of the different fibres joining the basal bodies of cells with more than two flagella could then lead to the complex synchronization patterns observed experimentally [40]. Yet, subtle hydrodynamic effects can exist, and need to be investigated through dedicated experiments blocking fluid-mediated coupling between flagella. These are currently underway.

With coordination of cilia and flagella within single cells being sensitive to the direct intracellular coupling between the filaments, we believe that better understanding its emergence will eventually enable synchronization to be used as a new and sensitive probe for the intracellular mechanical state of a cell.

DATA ACCESSIBILITY

Additional data are included in the electronic supplementary material.

AUTHORS' CONTRIBUTION

M.P. and D.R.B. designed the research; M.P., D.R.B., and R.C. developed the initial model; D.R.B. and Y.L. developed the full model and performed the simulations; M.P., D.R.B. and Y.L. analysed the data and wrote the manuscript.

COMPETING INTERESTS

We declare we have no competing interests.

FUNDING

This work was supported by: a Discovery Early Career Researcher Award (DECRA) from the Australian Research Council (D.R.B.); the University of Melbourne through an Albert Shimmins International Fellowship (M.P. and D.R.B.), and a Mathematics Vacation Scholarship (Y.L.).

ACKNOWLEDGEMENTS

M.P. gratefully acknowledges the hospitality of the School of Mathematics and Statistics from the University of Melbourne, where part of this work was done.

[1] Gray J, Hancock GJ. 1955 The propulsion of sea-urchin spermatozoa. *J. Exp. Biol.* **32**, 802–814.

[2] Nonaka S, Shiratori H, Saijoh Y, Hamada H. 2002 Determination of left–right patterning of the mouse embryo by artificial nodal flow. *Nature* **418**, 96–99. (doi:10.1038/nature00849)

[3] Hagenlocher C, Walentek P, Müller C, Thumberger T, Feistel K. 2013 Ciliogenesis and cerebrospinal fluid flow in the developing Xenopus brain are regulated by *foxj1*. *Cilia* **2**, 12. (doi:10.1186/2046-2530-2-12)

[4] Knight-Jones EW. 1954 Relations between metachronism and the direction of ciliary beat in metazoa. *Q. J. Microsc. Sci.* **95**, 503–521.

[5] Gueron S, Levit-Gurevich K. 1999 Energetic considerations of ciliary beating and the advantage of metachronal coordination. *Proc. Natl Acad. Sci. USA* **96**, 12240–12245. (doi:10.1073/pnas.96.22.12240)

[6] Tam D, Hosoi AE. 2011 Optimal feeding and swimming gaits of biflagellated organisms. *Proc. Natl Acad. Sci. USA* **108**, 1001–1006. (doi:10.1073/pnas.1011185108)

[7] Taylor GI. 1951 Analysis of the swimming of microscopic organisms. *Proc. R. Soc. Lond. A* **209**, 447–461. (doi:10.1098/rspa.1951.0218)

[8] Mettot C, Lauga E. 2011 Energetics of synchronized states in three-dimensional beating flagella. *Phys. Rev. E* **84**, 061905. (doi:10.1103/PhysRevE.84.061905)

[9] Michelin S, Lauga E. 2010 Efficiency optimization and symmetry-breaking in a model of ciliary locomotion. *Phys. Fluids* **22**, 111901. (doi:10.1063/1.3507951)

[10] Ding Y, Nawroth JC, McFall-Ngai MJ, Kanso E. 2014 Mixing and transport by ciliary carpets: a numerical study. *J. Fluid Mech.* **743**, 124–140. (doi:10.1017/jfm.2014.36)

[11] Goldstein RE, Polin M, Tuval I. 2009 Noise and synchronization in pairs of beating eukaryotic flagella. *Phys. Rev. Lett.* **103**, 168103. (doi:10.1103/PhysRevLett.103.168103)

[12] Uchida N, Golestanian R. 2011 Generic conditions for hydrodynamic synchronization. *Phys. Rev. Lett.* **106**, 058104. (doi:10.1103/PhysRevLett.106.058104)

[13] Geyer VF, Jülicher F, Howard J, Friedrich BM. 2013 Cell-body rocking is a dominant mechanism for flagellar synchronization in a swimming alga. *Proc. Natl Acad. Sci. USA* **110**, 18058-18063. (doi:10.1073/pnas.1300895110)

[14] Brumley DR, Wan KY, Polin M, Goldstein RE. 2014 Flagellar synchronization through direct hydrodynamic interactions. *eLife* **3**, e02750. (doi:10.7554/eLife.02750)

[15] Klindt GS, Ruloff C, Wagner C, Friedrich BM. 2017 In-phase and anti-phase flagellar synchronization by waveform compliance and basal coupling. *New J. Phys.* **19**, 113052. (doi:10.1088/1367-2630/aa9031)

[16] Rothschild, V. 1949 Measurement of sperm activity before artificial insemination. *Nature* **163**, 358–359.

[17] Riedel IH, Kruse K, Howard J. 2005 A self-organized vortex array of hydrodynamically entrained sperm cells. *Science* **309**, 300–303. (doi:10.1126/science.1110329)

[18] Bruot N, Cicuta P. 2016 Realizing the physics of motile cilia synchronization with driven colloids. *Annu. Rev. Condens. Matter Phys.* **7**, 323–348. (doi:10.1146/annurev-conmatphys-031115-011451)

[19] Brumley DR, Rusconi R, Son K, Stocker R. 2015 Flagella, flexibility and flow: Physical processes in microbial ecology. *Eur. Phys. J. Special Topics* **224**, 3119–3140. (doi:10.1140/epjst/e2015-50138-9)

[20] Vilfan A, Jülicher F. 2006 Hydrodynamic flow patterns and synchronization of beating cilia. *Phys. Rev. Lett.* **96**, 058102. (doi:10.1103/PhysRevLett.96.058102)

[21] Uchida N, Golestanian R. 2012 Hydrodynamic synchronization between objects with cyclic rigid trajectories. *Eur. Phys. J. E* **35**,135. (doi:10.1140/epje/i2012-12135-5)

[22] Brumley DR, Polin M, Pedley TJ, Goldstein RE. 2012 Hydrodynamic synchronization and metachronal waves on the surface of the colonial alga *Volvox carteri*. *Phys. Rev. Lett.* **109**, 268102. (doi:10.1103/PhysRevLett.109.268102)

[23] Lagomarsino MC, Jona P, Bassetti B. 2003 Metachronal waves for deterministic switching two-state oscillators with hydrodynamic interaction. *Phys. Rev. E* **68**, 021908. (doi:10.1103/PhysRevE.68.021908)

[24] Lenz P, Ryskin A. 2006 Collective effects in ciliar arrays. *Phys. Biol.* **3**, 285–294. (doi:10.1088/1478-3975/3/4/006)

[25] Wollin C, Stark H. 2011 Metachronal waves in a chain of rowers with hydrodynamic interactions. *Eur. Phys. J. E* **34**, 42. (doi:10.1140/epje/i2011-11042-7)

[26] Brumley DR, Bruot N, Kotar J, Goldstein RE, Cicuta P, Polin M. 2016 Long-range interactions, wobbles, and phase defects in chains of model cilia. *Phys. Rev. Fluids* **1**, 081201(R). (doi:10.1103/PhysRevFluids.1.081201)

[27] Kotar J, Leoni M, Bassetti B, Lagomarsino MC, Cicuta P. 2010 Hydrodynamic synchronization of colloidal oscillators. *Proc. Natl Acad. Sci. USA* **107**, 7669–7673. (doi:10.1073/pnas.0912455107)

[28] Di Leonardo R, Búzás A, Kelemen L, Vizsnyiczai G, Oroszi L, Ormos P. 2012 Hydrodynamic synchronization of light driven microrotors. *Phys. Rev. Lett.* **109**, 034104. (doi:10.1103/PhysRevLett.109.034104)

[29] Uchida N, Golestanian R. 2010 Synchronization and collective dynamics in a carpet of microfluidic rotors. *Phys. Rev. Lett.* **104**, 178103. (doi:10.1103/PhysRevLett.104.178103)

[30] Kotar J, Debono L, Bruot N, Box S, Phillips D, Simpson S, Hanna S, Cicuta P. 2013 Optimal hydrodynamic synchronization of colloidal rotors. *Phys. Rev. Lett.* **111**, 228103. (doi:10.1103/PhysRevLett.111.228103)

[31] Jeanneret R, Contino M, Polin M. 2016 A brief introduction to the model microswimmer *Chlamydomonas rein-*

hardtii. *Eur Phys. J. Special Topics* **225**, 2141–2156. (doi:10.1140/epjst/e2016-60065-3)

[32] Goldstein RE. 2015 Green algae as model organisms for biological fluid dynamics. *Annu. Rev. Fluid Mech.* **47**, 343–375. (doi:10.1146/annurev-fluid-010313-141426)

[33] Ringo DL. 1967 Flagellar motion and fine structure of the flagellar apparatus in *Chlamydomonas*. *J. Cell Biol.* **33**, 543–571. (doi:10.1083/jcb.33.3.543)

[34] Rüffer U, Nultsch W. 1998 Flagellar coordination in *Chlamydomonas* cells held on micropipettes. *Cell Motil. Cytoskeleton* **41**, 297–307. (10.1002/(SICI)1097-0169(1998)41:4<297::AID-CM3>3.0.CO;2-Y)

[35] Rüffer U, Nultsch W. 1987 Comparison of the beating of cis- and trans-flagella of *Chlamydomonas* cells held on micropipettes. *Cell Motil. Cytoskeleton* **7**, 87–93. (doi:10.1002/cm.970070111)

[36] Polin M, Tuval I, Drescher K, Gollub JP, Goldstein RE. 2009 *Chlamydomonas* swims with two "gears" in a eukaryotic version of run-and-tumble locomotion. *Science* **325**, 487–490. (doi:10.1126/science.1172667)

[37] Goldstein RE, Polin M, Tuval I. 2011 Emergence of synchronized beating during the regrowth of eukaryotic flagella. *Phys. Rev. Lett.* **107**, 148103. (doi:10.1103/PhysRevLett.107.148103)

[38] Son K, Brumley DR, Stocker R. 2015 Live from under the lens: exploring microbial motility with dynamic imaging and microfluidics. *Nat. Rev. Micro.* **13**, 761–775. (doi:10.1038/nrmicro3567)

[39] Quaranta G, Aubin-Tam M-E, Tam D. 2015 Hydrodynamics versus intracellular coupling in the synchronization of eukaryotic flagella. *Phys. Rev. Lett.* **115**, 238101. (doi:10.1103/PhysRevLett.115.238101)

[40] Wan KY, Goldstein RE. 2016 Coordinated beating of algal flagella is mediated by basal coupling. *Proc. Natl Acad. Sci. USA* **113**, E2784–E2793. (doi:10.1073/pnas.1518527113)

[41] Leptos KC, Wan KY, Polin M, Tuval I, Pesci AI, Goldstein RE. 2013 Antiphase synchronization in a flagellar-dominance mutant of *Chlamydomonas*. *Phys. Rev. Lett.* **111**, 158101. (doi:10.1103/PhysRevLett.111.158101)

[42] Wright RL, Chojnacki B, Jarvik JW. 1983 Abnormal basal-body number, location, and orientation in a striated fiber-defective mutant of *Chlamydomonas reinhardtii*. *J. Cell Biol.* **96**, 1697–1707. (doi:10.1083/jcb.96.6.1697)

[43] Kamm RD. 2015 *Mechanics of the Cytoskeleton*, MIT OpenCourseWare.

[44] Niedermayer T, Eckhardt B, Lenz P. 2008 Synchronization, phase locking, and metachronal wave formation in ciliary chains. *Chaos* **18**, 037128. (doi:10.1063/1.2956984)

[45] Rüffer U, Nultsch W. 1997 Flagellar photoresponses of *ptx1*, a nonphototactic mutant of *Chlamydomonas*. *Cell Motil. Cytoskeleton* **37**, 111–119. (doi:10.1002/(SICI)1097-0169(1997)37:2<111::AID-CM3>3.0.CO;2-B)

[46] Inouye I. 1993 Flagella and flagellar apparatuses of algae. *Ultrastructure of Microalgae*, CRC Press. 99–133.

[47] Landau LD, Lifshitz EM. 1986 *Theory of elasticity, 3rd edition (course of theoretical physics, vol. 7)*. Oxford, UK: Butterworth-Heinemann.

[48] Strogatz SH. 1994 *Nonlinear dynamics and chaos*. Cambridge, MA: Perseus Books Publishing, LLC.

[49] Röhm A, Lüdge K, Schneider I. 2018 Bistability in two simple symmetrically coupled oscillators with symmetry-broken amplitude- and phase-locking. *Chaos* **28**, 063114. (doi:10.1063/1.5018262)

[50] Banerjee T, Biswas D, Ghosh D, Bandyopadhyay B, Kurths J. 2018 Transition from homogeneous to inhomogeneous limit cycles: Effect of local filtering in coupled oscillators. *Phys. Rev. E* **97**, 042218. (doi:10.1103/PhysRevE.97.042218)

[51] Scheffer M, Bascompte J, Brock WA, Brovkin V, Carpenter SR, Dakos V, Held H, Van Nes EH, Rietkerk M, Sugihara G. 2009 Early-warning signals for critical transitions. *Nature* **461**, 53-59. (doi:10.1038/nature08227)

[52] Thompson JMT, Sieber J. 2011 Predicting climate tipping as a noisy bifurcation: a review. *International Journal of Bifurcation and Chaos* **21**, 399–423. (doi:10.1142/S0218127411028519)

[53] Miller NJ, Shaw SW. 2012 Escape statistics for parameter sweeps through bifurcations. *Phys. Rev. E* **85**, 046202. (doi:10.1103/PhysRevE.85.046202)

[54] Herbert C, Bouchet F. 2017 Predictability of escape for a stochastic saddle-node bifurcation: When rare events are typical. *Phys. Rev. E* **96**, 030201(R). (doi:10.1103/PhysRevE.96.030201)

[55] Elgeti J, Gompper G. 2013 Emergence of metachronal waves in cilia arrays. *Proc. Natl Acad. Sci. USA* **110**, 4470–4475. (doi:10.1073/pnas.1218869110)

[56] Harris EH, Stern DB, Witman GB. 2009 *The chlamydomonas sourcebook, vol. 1*. San Diego, CA: Elsevier.

[57] Collingridge P, Brownlee C, Wheeler GL. 2013 Compartmentalized calcium signaling in cilia regulates intraflagellar transport. *Current Biology* **23**, 2311–2318. (doi:10.1016/j.cub.2013.09.059)

[58] Wheeler GL, Joint I, Brownlee C. 2008 Rapid spatiotemporal patterning of cytosolic Ca^{2+} underlies flagellar excision in *Chlamydomonas reinhardtii*. *Plant J.* **53**, 401–413. (doi:10.1111/j.1365-313X.2007.03349.x)

[59] Wheeler GL, Brownlee C. 2008 Ca^{2+} signalling in plants and green algae – changing channels. *Trends Plant Sci.* **13**, 506–514. (doi:10.1016/j.tplants.2008.06.004)